

# Journal of Materials Chemistry A

Accepted Manuscript

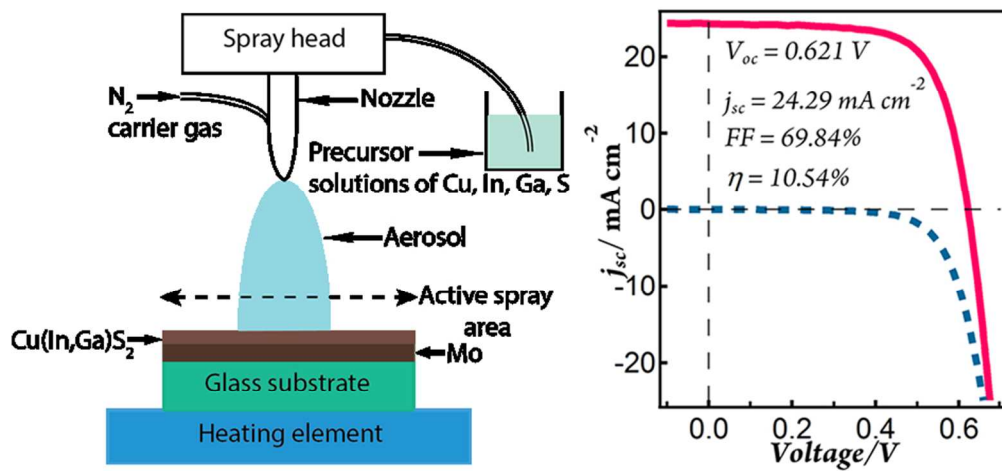


This is an *Accepted Manuscript*, which has been through the Royal Society of Chemistry peer review process and has been accepted for publication.

*Accepted Manuscripts* are published online shortly after acceptance, before technical editing, formatting and proof reading. Using this free service, authors can make their results available to the community, in citable form, before we publish the edited article. We will replace this *Accepted Manuscript* with the edited and formatted *Advance Article* as soon as it is available.

You can find more information about *Accepted Manuscripts* in the [Information for Authors](#).

Please note that technical editing may introduce minor changes to the text and/or graphics, which may alter content. The journal's standard [Terms & Conditions](#) and the [Ethical guidelines](#) still apply. In no event shall the Royal Society of Chemistry be held responsible for any errors or omissions in this *Accepted Manuscript* or any consequences arising from the use of any information it contains.



An aqueous spray-pyrolysis approach for synthesizing Cu(In,Ga)(S,Se)<sub>2</sub> thin film which leads to 10.54% power conversion efficiency in solar cell, and shows ease of fabrication of films in large-scale at much cheaper cost.

80x39mm (300 x 300 DPI)

## Synthesis of Cu(In,Ga)(S,Se)<sub>2</sub> thin films using an aqueous spray-pyrolysis approach, and their solar cell efficiency of 10.5%.

*Md. Anower Hossain<sup>a</sup>; Zhang Tianliang<sup>a</sup>; Lee Kian Keat<sup>a</sup>, Li Xianglin<sup>a</sup>; Rajiv R. Prabhakar<sup>a</sup>; Sudip K. Batabyal<sup>a</sup>, Subodh G. Mhaisalkar<sup>ab</sup>, and Lydia H. Wong<sup>ab\*</sup>.*

---

<sup>a</sup> Energy Research Institute @ NTU (ERI@N), Nanyang Technological University, Singapore.

<sup>b</sup> School of Materials Science & Engineering, Nanyang Technological University, Singapore.

\*email: LydiaWong@ntu.edu.sg

## Abstract

Semiconducting  $\text{Cu(In,Ga)(S,Se)}_2$  (CIGSSe) thin-film is prepared by spray-pyrolysis of aqueous precursor solutions of copper ( $\text{CuCl}_2$ ), indium ( $\text{InCl}_3$ ), gallium ( $\text{GaCl}_3$ ), and sulphur ( $\text{SC(NH}_2)_2$ ) sources. The non-vacuum approach of making the CIGSSe thin film using environmentally benign halide-based aqueous precursor solutions paves the way of fabricating solar cells at much cheaper cost. Here, gallium (Ga) is incorporated into the host lattice of  $\text{CuIn(S,Se)}_2$  (CISSe) films grown on Mo-coated soda-lime glass substrate to modify the optoelectronic properties of CIGSSe films. The bandgap engineered, Ga-doped CIGSSe film leads to better photovoltaic characteristics and shows one of the highest efficiency CIGS thin film solar cell made by non-vacuum deposition of environmentally-friendly precursors. The optimum efficiency of solar cells with the device configuration of glass/Mo/CIGSSe/CdS/i-ZnO/AZO show  $j$ - $V$  characteristics of  $V_{oc} = 0.621$  V,  $j_{sc} = 24.29$  mA  $\text{cm}^{-2}$ ,  $FF = 69.84$  %, and power conversion efficiency of 10.54% under simulated AM 1.5  $100$  mW  $\text{cm}^{-2}$  illuminations, demonstrating its potential in making a cost-effective thin film solar cell.

## Introduction

Thin film solar technologies have the potential in producing cost-effective solar cells. Nowadays, chalcopyrite  $\text{Cu}(\text{In,Ga})\text{Se}_2$  (CIGS)-based thin film solar cells show power conversion efficiency (PCE) of up to 20.9%.<sup>1, 2</sup> However, they require complex deposition processes involving costly vacuum technologies to sputter or co-evaporate constituents of the CIGS thin films.<sup>2, 3</sup> Although they show excellent PCE in solar cells, the preparation approach involves expensive instrumentation and toxic post-selenization step, *i.e.*, in  $\text{H}_2\text{Se}$  gas, thus raising the production cost of solar cells.<sup>4</sup> In this regards, a non-vacuum solution-based CIGS thin film preparation approach has shown ability to avoid the issues related to the toxicity and high production cost as it requires inexpensive instruments and non-/less-toxic precursor materials. Very recently, the solution-processed spray-coating approach has been utilized to grow  $\text{CH}_3\text{NH}_3\text{PbI}_{3-x}\text{Cl}_x$  perovskite material for planar heterojunction solar cells, suggesting the potential of this approach for fabricating efficient large-area solar cell at much cheaper cost.<sup>5</sup>

Till date, many solution-based chemical approaches have been utilized to prepare CIGS thin films.<sup>6-14</sup> In the reported methods, precursors of copper (Cu), indium (In), gallium (Ga) and sulphur (S) have been utilized to prepare the CIGS films. However, their photovoltaic performance was limited by poor crystallinity of the films and presence of various impurities which resulted in low open circuit voltage ( $V_{oc}$ ), and short-circuits photocurrent density ( $j_{sc}$ ). The commonly used solution-based approaches are spray-pyrolysis of precursor solution,<sup>6, 9, 15</sup> spin-coating of molecular precursors,<sup>16-22</sup> and use of pre-synthesized nanoparticles.<sup>23-28</sup> Among these, the decomposition of  $\text{Cu}_2\text{S}$ ,  $\text{In}_2\text{Se}_3$ , and  $\text{Ga}_2\text{S}_3$  in hydrazine has demonstrated the highest known 15.2% efficient solution processed thin film solar cells.<sup>21, 29</sup> However, hydrazine-based synthesis approach may not be suitable in an industrial production line because of its toxicity and explosive nature. Additionally, the spray-pyrolysis and spin-coating approaches showed carbonaceous impurities in the CIGS films, especially when alcohols were used to dissolve the halide and/or nitrate-based precursors of Cu, In, and Ga.<sup>30, 31</sup> The carbonaceous impurity affects the crystal growth of CIGS films and acts as barrier for charge extraction in solar cell.

To evade the above issues of toxicity and impurity, our group has reported  $\text{CuIn}(\text{S,Se})_2$  (CISSe) films prepared by spray-pyrolysis of aqueous  $\text{CuCl}_2$ ,  $\text{InCl}_3$ , and thiourea precursor solution on molybdenum (Mo) substrate and subsequent selenization.<sup>32</sup> The usage of water as

solvent and non-toxic chemicals made the CuInS<sub>2</sub> (CIS) film preparation approach environmentally benign and facile. Additionally, the use of water as solvent allowed the CISSe films to be free from carbonaceous impurities. However, the reported efficiency of the CISSe film-based solar cells showed PCE of 5.9% only, in which the PCE was found to be affected by low  $V_{oc}$  and fill factor ( $FF$ ).<sup>32</sup> To enhance the  $V_{oc}$  of solar cells, doping of the CIS films with Ga is widely used to enhance the optoelectronic properties (*i.e.*, bandgap energy ( $E_g$ ), charge carrier mobilities and concentrations, *etc.*).<sup>33</sup> Depending on the concentration of Ga dopants, the  $E_g$  can be systematically increased from 1.05 eV (CuInSe<sub>2</sub>) to 1.2-1.5 eV Cu(In,Ga)(S, Se)<sub>2</sub> (CIGSSe) which directly improves the efficiency of solar cells by improving the  $V_{oc}$  and  $FF$ . In this study, using a non-vacuum spray-pyrolysis method and subsequent selenization step, different amounts of Ga dopant are systematically incorporated into the CISSe film to obtain the CIGSSe films with favourable optoelectronic properties. An optimized CIGSSe film prepared by spray-pyrolysis of metal halide precursors and thiourea solution onto Mo-coated soda-lime glass (SLG) substrate at 300-350 °C and subsequent selenization at 500 °C leads to a PCE of 10.54%. This efficiency of CIGSSe-based solar cell is one of the highest among the solution-processed thin film solar cells. A combination of XRD, Raman and FE-SEM analyses show that the properties of the CIGSSe thin films can favourably be changed with successful Ga doping, which ultimately contribute to higher  $V_{oc}$ , and  $FF$ ; thus the increased PCE of solar cells.

## Experiments

**Preparation of molybdenum (Mo) substrate.** SLG substrate was cleaned by sequential sonication in 5% Decon 90 aqueous solution at 60 °C for 30 minutes followed by rinsing with deionized (DI) water and drying in N<sub>2</sub> stream. To further remove the water residue from dried SLG, they were finally dried in an electric oven at 70 °C for 15 minutes. Following this, a Univex 350 sputtering system was used to deposit the Mo film on the SLG, in which the surface of the SLG was further cleaned by argon plasma source generated at 200 W. The operating pressure of the deposition chamber was approximately,  $7 \times 10^{-6}$  mbar. Single and Bi-layer Mo film of approximately 1 μm thickness was deposited onto the SLG substrate with DC bias at 360 W. To avoid oxidation of as-deposited thin film Mo, it was naturally cooled down to room temperature inside the deposition chamber before being taken out to air.

**Preparation of light absorbing thin films.** The Mo-coated SLG substrate was cleaned by sequential sonication with aqueous solution of 2.5% hellmanex-III for 5 minutes followed by in a mixture of ethanol and deionized water, and finally in deionized water for 10 minutes each. Following this, they were dried in N<sub>2</sub> stream prior to deposition of CIS and CIGS films. Aqueous 0.2 M copper (II) chloride dihydrate (CuCl<sub>2</sub>·2H<sub>2</sub>O, 99.99% Aldrich), 0.2 M indium (III) chloride (InCl<sub>3</sub>, anhydrous 99.999%, Aldrich), 0.2 M gallium (III) chloride (GaCl<sub>3</sub>, anhydrous 99.999% Aldrich), and 1 M thiourea (SC(NH<sub>2</sub>)<sub>2</sub>, 99.0%, Sigma Aldrich) were prepared and used as stock solution. Diluted aqueous solutions were prepared by keeping the volume of Cu and S precursor's stock solution constant, but varying the volume of In and Ga precursors to change the composition of sprayed CIS and CIGS films. The similar graded spray-pyrolysis approach was reported earlier by our group.<sup>32</sup> In brief, the precursor solution was sprayed onto the cleaned Mo substrate at temperature of 300-350 °C using an air brush with N<sub>2</sub> as carrier gas at 4 bars in a fume hood.

The thin films were prepared using with and without Ga variations by maintaining the Ga/(In+Ga) = 0.00 for CIS and Ga/(In+Ga) = 0.15, 0.20, 0.25 and 0.30 for CIGS. The CIS thin film was used to compare the performance of the CIGS films. The precursor material decomposes on Mo substrate during the deposition temperature at 300-350 °C and the resulted film is often amorphous or nanocrystalline and may include impurity phases.<sup>32</sup> Therefore, the as-sprayed CIS and CIGS films were selenized in an argon filled selenization tube furnace (Thermo Scientific, single zone) to allow the grain growth and densification of the films by taking 30 mg of selenium (Se) pellet in a quartz tube at an optimized temperature of 500 °C for 10 minutes. After selenization the CIS and CIGS films transform to CuIn(S,Se)<sub>2</sub> (CISSe) and Cu(In,Ga)(S,Se)<sub>2</sub> (CIGSSe). The selenization parameters include Se evaporation temperature, flow rate of argon carrier gas, and selenization time. Beside the grain growth, the selenization condition also simultaneously reduces defect states at the inter-crystalline boundary regions. Following the selenization step, they were cooled down to room temperature and immediately transferred from tube furnace into the preheated chemical bath deposition of CdS.

**Characterization of thin films.** The crystal structure of the as-sprayed and selenized films were characterized by means of X-ray diffraction (XRD) technique with a Bruker D8 advance diffractometer using Cu K<sub>α1</sub> radiation ( $\lambda = 0.1541$  nm). The microstructure of CISSe and CIGSSe films were characterized by field-emission scanning electron microscope (FESEM, JEOL JSM-7600F). Prior to electron microscopy, a thin Pt layer was deposited to

prevent charging effects. Energy-dispersive X-ray spectroscopy (EDS) elemental analysis of the films was carried out using the above FESEM fitted with EDS analyser. Raman spectroscopy measurement was carried out with a micro-Raman spectrometer (Renishaw system) in backscattering configuration using a diode-pumped solid state laser with 532 nm and with an excitation power of 1 mW. The carrier mobility and concentration in the films were estimated using a temperature variable Hall measurement system (MMR technologies). The films were prepared on glass substrates with an area of 1 cm<sup>2</sup> and four aluminum square electrodes (1.6 mm x 1.6 mm) were thermally evaporated. The Hall measurements were carried out at room temperature (302 K).

**Fabrication of solar cells.** To fabricate the heterojunction thin film solar cells with *p*-type CIGSSe films, an n-type CdS buffer layer of approximately 50 nm thickness was deposited onto the CISSe and CIGSSe films by chemical bath deposition. The temperature of water bath was 80 °C and the thin films were placed in 200 ml aqueous solution that contains 4 mM cadmium acetate hydrate (Cd(CH<sub>3</sub>COO)<sub>2</sub>, 99.00%, Aldrich), 4 mM ammonium acetate (NH<sub>4</sub>(CH<sub>3</sub>COO), 99.99%, Sigma Aldrich), 2 mM thiourea (SC(NH<sub>2</sub>)<sub>2</sub>, 99.0%, Sigma Aldrich), and 0.3 ml ammonium hydroxide solution (NH<sub>4</sub>OH, 28-30% solution, Sigma Aldrich). After CdS deposition for 11 minutes, the thin films were rinsed with deionized water and immediately dried in N<sub>2</sub> stream. Following this, approximately a 50 nm thick intrinsic zinc oxide (*i*-ZnO) and 500 nm thick aluminium-doped ZnO (AZO) were deposited by the Univex 350 sputtering system with RF power of 100 W for 10 min and 160 W for 120 min, respectively. Finally, to collect photogenerated charge carriers and reduce the series resistance, a patterned top electrode made of Ni/Al was thermally evaporated onto the above electrodes using aluminium (Al) and nickel (Ni) pellets as evaporation source. Following this, they were mechanically scribed to define the active area of individual solar cells to be 0.1 cm<sup>2</sup>.

**Characterization of solar cells.** A solar simulator (VS-0852) was utilized to measure the *j*-*V* characteristics of solar cells under the simulated AM 1.5 100 mW cm<sup>-2</sup> illumination using a Keithley Source (2612A) meter and IV tester software package. The solar simulator was equipped with a 500 W xenon lamp and the light intensity was calibrated using Si reference solar cell (Fraunhofer). Incident photon to current efficiency (IPCE) spectra was measured with a spectral resolution of *ca.* 5 nm using a PVE300 photovoltaic device characterization system (Bentham) equipped with a xenon/quartz lamp. The incident photon flux was determined using calibrated silicon (Si) and germanium (Ge) photodiodes which allowed us

to measure the IPCE up to photon wavelength of 1800 nm. Controlling of the monochromator and recording of photocurrent spectra were performed using a PC running Bentham software package.

## Results and Discussion

**Structural and morphological characterizations of thin films.** The as-sprayed CIS, CIGS and selenized CISSe, CIGSSe films were characterized by glancing angle XRD with an incident angle of one degree as shown in Figure 1. The XRD patterns of as-sprayed films show characteristic diffraction peaks, indicating the presence of polycrystalline CIS material (Fig. 1(a)). They show XRD peaks with broad full width half maximum (FWHM) and low intensities, suggesting poor crystallinity of as-sprayed films. The XRD patterns of as-sprayed films confirm the absence of crystalline impurity phases of  $\text{Cu}_{2-x}\text{S}$ ,  $\text{MoO}_2$ , and  $\text{MoS}_2$  (Fig. 1(a)).

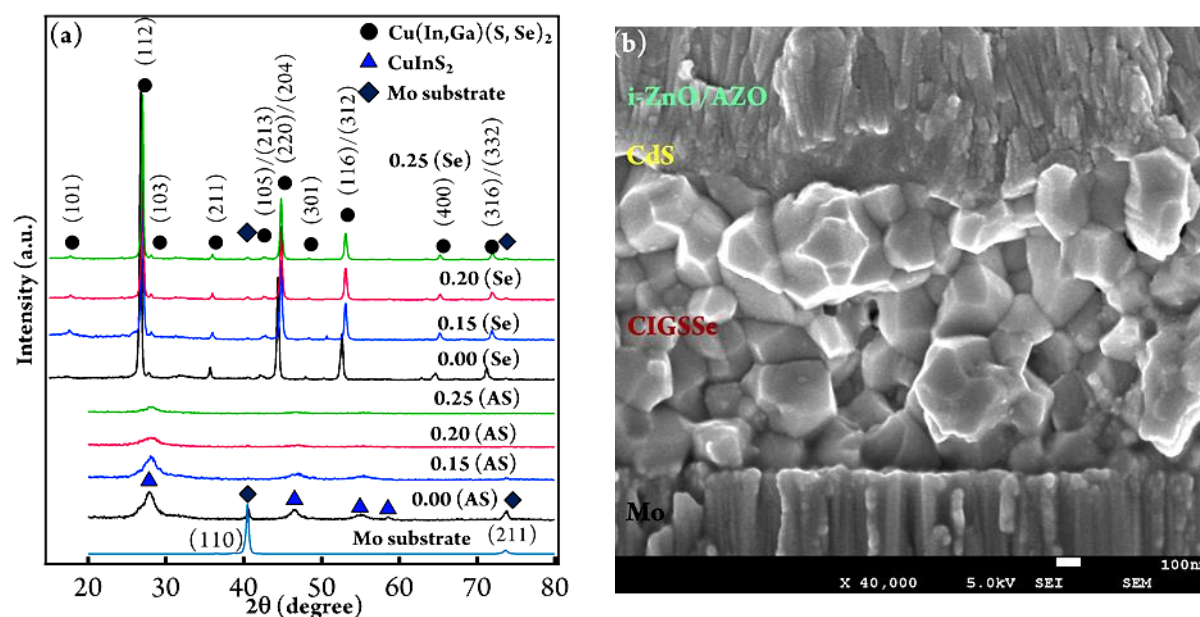


**Figure 1.** (a) XRD patterns of CIS, CIGS, CISSe, and CIGSSe thin films prepared on Mo-coated SLG substrate with different Ga/(In+Ga) ratio of 0.00, 0.15, 0.20, and 0.25. The words, AS and Se in bracket refers to as-sprayed and selenized films, respectively. The XRD pattern of Mo-coated SLG substrate is also included for reference. Figure 1(b) shows cross-sectional image of a CIGSSe solar cell.

The Ga incorporation during selenization step at 500 °C causes shift of XRD patterns of the CIGSSe films towards higher  $2\theta$  with respect to that of the CISSe film, indicating successful Ga doping into CISSe films (atomic size of Ga is smaller than In). The incorporation of Se into the as-sprayed CIS and CIGS films during selenization (Se has larger atom size than S) causes the lattice expansion of CISSe and CIGSSe films; thus their XRD patterns are left-shifted as compared to the as-sprayed films (Fig. 1(a)). To ensure that the amount of lattice expansion due to selenization is similar in all films, the Cu/S in the as-sprayed films was kept constant (using the same amount of Cu and S precursor solutions) and the same selenization condition was used for all films. Therefore, the right shift of the CIGSSe film is purely attributed to the effect of Ga substitution in In lattice. The lattice parameters of these films were also determined by profile fitting (Rietveld refinement) of the full XRD patterns, which show that as compared to the CISSe film the unit cell parameters  $a$ ,  $c$  and volume ( $V$ ) of tetragonal body centered CIGSSe films progressively reduces with increasing Ga content as shown in Table 1. These unit cell parameters also confirm the partial substitution of bigger In atoms by smaller Ga in CIGSSe films.

**Table 1.** Rietveld refinement results of the CISSe and CIGSSe films.

<i>Thin films</i>	<i>Ga/(In+Ga)</i>	<i>a (Å)</i>	<i>c (Å)</i>	<i>V (Å<sup>3</sup>)</i>
CISSe	0.00	5.757	11.575	383.62
CIGSSe	0.15	5.730	11.542	378.96
	0.20	5.703	11.471	373.08
	0.25	5.700	11.461	372.39

In case the XRD peaks of the films interfere with the possible impurities related to Mo, such as Mo metal, MoS<sub>2</sub>, and MoSe<sub>2</sub>, the thin films were simultaneously deposited onto glass substrate, which show the same right-shifted XRD patterns (supporting information, Figure S1). The XRD peaks corresponding to Cu-Se compounds (*e.g.*, Cu<sub>2-x</sub>Se) were not observed in the CISSe and CIGSSe films as they are less prone to form in Cu-poor condition.<sup>34</sup> The Cu-deficient CIGS inhibits the formation of detrimental Cu<sub>2</sub>S at the heterojunction interface of CdS and CIGSs. Figure 1(b) shows cross-sectional FESEM image of the CIGSSe solar cell. The size of crystal grains is found to be 300-500 nm with film thickness of approximately

1.15  $\mu\text{m}$ . A conformal CdS layer with a thickness of approximately 50 nm can be seen on top of the CIGSSe film (Fig. 1(b)). It should be noted that the as-sprayed CIS and CIGS films are polycrystalline with grain size in the range of 20-40 nm.<sup>32</sup> The high surface energy of the small grains is believed to be beneficial for incorporation of selenium ( $\text{Se}^{2-}$ ) vapor during selenization at 500 °C. The microstructural change of the CISSe and CIGSSe films usually depends on selenization temperature which was kept constant at 500 °C for all of the films.<sup>35</sup> While the selenization recipe was same, it was observed that the grain size of the CIGSSe films was reduced with increasing Ga incorporation which is in agreement with previous reports.<sup>36-38</sup> The densification process was also discussed in the previous report by Ho *et al.*<sup>32</sup> As an example, the CIGSSe film with  $\text{Ga}/(\text{In}+\text{Ga}) = 0.30$  as shown in Figure S2 (supporting information) has smaller crystal grains than that of the CIGSSe film with  $\text{Ga}/(\text{In}+\text{Ga}) = 0.20$  (Figure 1(b)). Therefore, the grain size and densification of the CIGSSe films as well as the structural properties were affected by the incorporation of Ga, which impact negatively the performance of solar cells.<sup>39</sup>

**Raman studies.** Raman spectroscopy measurement was conducted using a micro-Raman at room temperature to further check the crystal quality and phase purity of the films (Fig. 2). The as-sprayed films (Fig. 2(a)) show the dominant  $A_1$  phonon mode at  $295\text{ cm}^{-1}$  ( $294\text{ cm}^{-1}$  for pure CIS) which indicates CIS phase.<sup>40</sup> The  $A_1$  mode is broad, suggesting amorphous nature of the Cu-deficient films that is consistent with the deposition condition, as all the as-sprayed CIS and CIGS films were removed from hotplate immediately after spraying of precursor solutions without further annealing. The slightly higher but similar  $A_1$  mode at  $295\text{ cm}^{-1}$  for all films (Fig. 2(a)) are due to the presence of Ga in the as-sprayed CIGS films, suggesting that the pyrolysis temperature of 300-350 °C is not sufficient for the Ga to be incorporated into the host lattice of CIS films. The shoulder peak at  $338\text{ cm}^{-1}$  could be the  $E_{\text{LO}}$  mode of CIS. The Raman spectra do not show impurity phases, such as CuS,  $\text{Cu}_{2-x}\text{S}$ , *etc.*

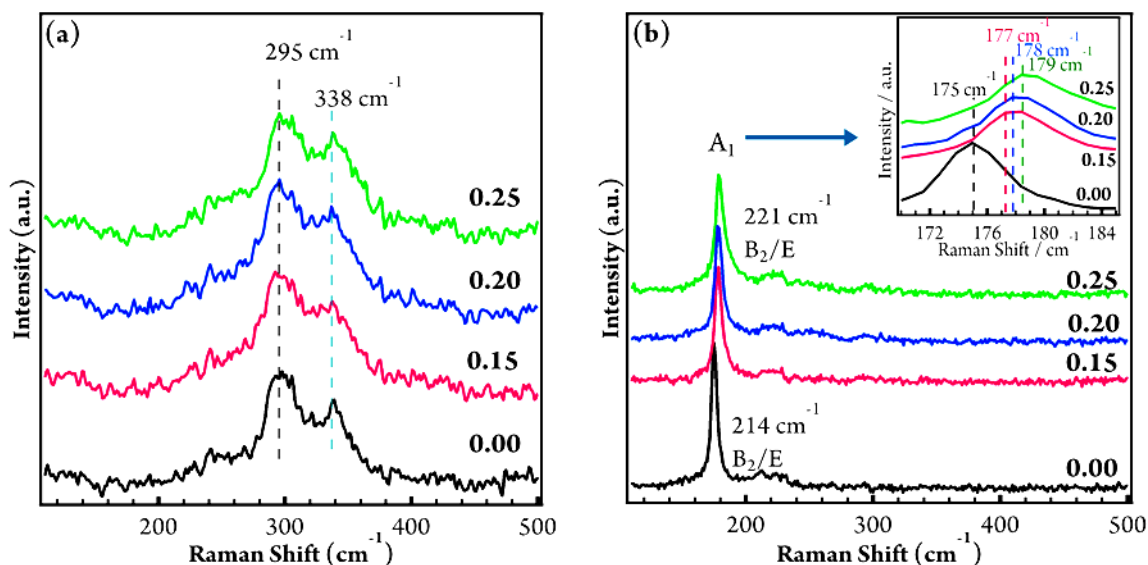


**Figure 2.** Raman spectra of as-prepared CIS and CIGS (a), and selenized CISSe and CIGSSe (b) films with different Ga/(In+Ga) ratio of 0.00, 0.15, 0.20 and 0.25 on Mo-coated SLG substrate. The inset of Figure 2(b) shows the right-shifted  $A_1$  mode of the films with increasing Ga content.

Figure 2(b) shows the dominant  $A_1$  mode at  $174\text{ cm}^{-1}$  for the CISSe film, which represents the vibration of Se anions in the x-y plane while cations remains at rest.<sup>41</sup> However, the frequency of  $A_1$  mode is increased to  $177\text{-}179\text{ cm}^{-1}$  (inset of Fig. 2(b)) with Ga incorporation into CIGSSe films, which is consistent with the linear increase of  $A_1$  mode with Ga content.<sup>42, 43</sup> It can also be seen that the intensity of  $A_1$  mode decreases with increasing Ga/(In+Ga) ratio, which is consistent with published data.<sup>44</sup> These films also show mixed  $B_2/E$  modes at  $214\text{ cm}^{-1}$  for CISSe film and approximately at  $221\text{ cm}^{-1}$  corresponding to CIGSSe films. The missing vibrational mode at  $260\text{ cm}^{-1}$  indicates the absence of  $A_1$  mode of Cu-Se compounds, such as  $\text{Cu}_{2-x}\text{Se}$ ,  $\text{CuSe}$  and  $\text{Cu}_3\text{Se}_2$ , further supporting XRD results (Fig. 1(a)) that the CISSe and CIGSSe films are single phase. The missing broad vibrational mode at  $150\text{ cm}^{-1}$  indicates that there are no order defects compound phases of  $\text{Cu}(\text{In,Ga})_3(\text{S,Se})_5$  or  $\text{Cu}_2(\text{In,Ga})_4(\text{S,Se})_7$  which are usually observed in Cu-poor CIGS films, especially when the  $\text{Cu}/(\text{In+Ga}) < 0.80$ , further confirming that our CISSe and CIGSSe films possess the  $\text{Cu}/(\text{In+Ga})$  values higher than 0.80 and validating the EDS elemental analysis (supporting information, Table 1).<sup>45</sup> These impurity-free and Cu-poor optimized CISSe and CIGSSe films were used to fabricate the solar cells.

**Compositional analysis of thin films.** EDS elemental analysis was conducted to determine the composition of CISSe and CIGSSe films. With an uncertainty of <0.1 wt% of the EDS measurement, it shows the Cu/In of CISSe and Cu/(In+Ga) of CIGSSe films approximately 0.85 (supporting information, Table 1) which is considered an optimum composition of thin films for high performance CIGS solar cells. It also suggests that there is no loss of In in the form of volatile  $\text{In}_2\text{Se}$  during the selenization step.<sup>46</sup> The benefits of the Cu-poor films are two-folds: firstly, formation of highly conductive detrimental impurity phases of  $\text{Cu}_{2-x}\text{Se}$ ,  $\text{Cu}_3\text{Se}_2$ , and  $\text{CuSe}$  can be avoided; thus post-treatment step in toxic KCN is not required.<sup>13</sup> Secondly, the semiconducting properties, such as charge carrier mobility and carrier concentration ( $1 \times 10^{16} \text{ cm}^{-2}$ ) become more favourable for solar cell applications.<sup>33, 47</sup> It is worth noting that despite spraying of the metal chloride aqueous precursor solution at a rate that allows sufficient time for chlorine (Cl) to escape with  $\text{N}_2$  gas in the form of HCl, Cl in the CISSe film was previously observed by wavelength-dispersive X-ray spectroscopy.<sup>32</sup> The high nucleophilic strength of  $\text{Cl}^-$  with metal cations implies that a larger supply of thermal energy is required to decompose anions for generating a pure CISSe and CIGSSe films.<sup>48</sup> It has been recently shown by thermo gravimetric analysis that  $\text{Cl}^-$ -containing CIGS ink continued weight loss until 650 °C. This indicates that the temperature of 400 °C to deposit the CIS, CIGS during spray-pyrolysis and their selenization at 500 °C to get CIGSSe films do not completely remove the  $\text{Cl}^-$  impurities.<sup>49</sup> More careful investigation on the role of  $\text{Cl}^-$  is required to understand its influence on grain growth and device properties.

**Photovoltaic characteristics.** To investigate the photovoltaic performance of the sprayed films, solar cells were fabricated with different Ga content and characterized as shown in Table 2. As expected, the  $V_{\text{oc}}$  of solar cells was found to increase with progressive Ga incorporation into the CIGS film. However, the increase in  $V_{\text{oc}}$  is dependent on the Ga/(In+Ga) ratio, which began to level out and eventually approached a saturation value of approximately 0.62 V. On contrary, the  $j_{\text{sc}}$  was found to decrease almost linearly with the increasing Ga content in the film which is consistent with the progressive blue-shifted onsets of IPCE spectra (Fig. 3(a)). The CISSe thin film was used as reference showing the highest  $j_{\text{sc}}$  but the lowest  $V_{\text{oc}}$  and  $FF$ . It has been reported that the Ga incorporation reduces the electrical resistivity of the CIGS film while the carrier concentration remains fairly constant up to Ga/(In+Ga) of 0.30.<sup>33</sup> The incorporated Ga also diffuses toward the back contact, creating a bandgap graded CIGS film that generates back surface field which greatly suppresses the back contact recombination and increases the  $V_{\text{oc}}$  of solar cells.<sup>50</sup> It has also

been reported that charge carrier mobility of the CIGS film enhances with the Ga/(In+Ga) ratio of up to 0.40 while the carrier concentration remains almost same.<sup>33</sup>

Therefore, with the increase of Ga/(In+Ga) ratio, the charge carrier separation and collection of the CIGSSe film are expected to be improved and result in higher  $V_{oc}$  and FF. The IPCE spectra show photocurrent response of solar cells made of the CISSe and CIGSSe films (Fig. 3(a)). As the Ga in the CIGSSe films increases, the onsets of IPCE spectra were shifted towards shorter wavelength resulting in a drop of  $j_{sc}$  (Fig. 3(b)). Despite the  $j_{sc}$  drop, the  $V_{oc}$  and FF increments result in an improved PCE. At an optimum value of Ga/(In+Ga) = 0.20 the PCE of the solar cells are 8.15% (Table 2). At this optimum value of Ga/(In+Ga) = 0.20, the  $E_g$  of our CIGSSe film was calculated to be 1.28 eV, ~~and the hole mobility and moderate carrier concentration were measured to be  $1 \text{ cm}^2 \text{ V}^{-1} \text{ s}^{-1}$  and  $1.6 \times 10^{15} \text{ cm}^{-3}$ , respectively, by Hall measurements.~~<sup>33</sup> ~~The measured hole mobility and carrier concentration was in fact found to be one order lower than the evaporation-based high efficiency CIGS film.~~<sup>47, 51</sup> Additionally, ~~the lower carrier concentration and mobility than that in the evaporation-based CIGS films could be attributed to the presence of S.~~

The efficiency of solar cells drops when Ga/(In+Ga) > 0.20 mostly due to reduced crystallinity of the CIGSSe film (Table 2). Much reduced crystal grains can be observed when the film has Ga/(In+Ga) of 0.30 (supporting information, Figure S2), which may affect charge transport properties of the resulting CIGSSe films. As a result, as shown in Figure 3(a) the peak IPCE of solar cells drop when the Ga/(In+Ga) > 0.20, implying that beyond this value the charge separation and collection becomes inefficient. It should be noted that the bandgap of the best reported CIGS solar cell deposited by co-evaporation is 1.15eV, and by hydrazine-based method is 1.16 eV, which means that with further optimization, we may be able to improve the efficiency of our solar cell.<sup>29, 39</sup> The higher  $E_g$  of our film may be caused by the high amount of S existing in the CIGSSe film (Table S1).

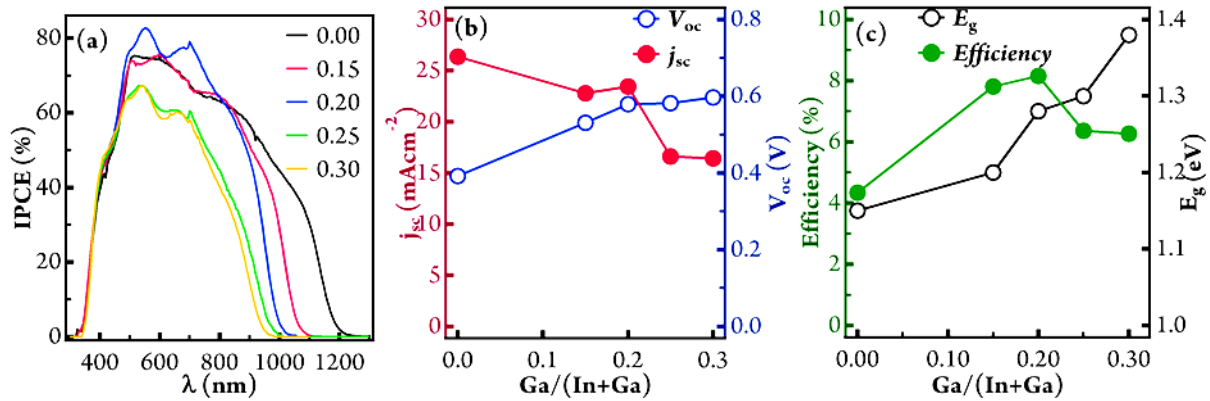


**Figure 3.** Shows  $j$ - $V$  characteristics of solar cells made of CISSe and CIGSSe films containing the Ga/(In+Ga) of 0.00, 0.15, 0.20, 0.25 and 0.30. The IPCE spectra (a) shows blue-shifted onsets of IPCE spectra with progressive Ga increment in thin films, the  $j_{sc}$  and  $V_{oc}$  (b) shows opposite trend with Ga/(In+Ga), and (c) efficiency and  $E_g$  variation with Ga/(In+Ga).

**Table 2.**  $j$ - $V$  characteristics of CISSe and CIGSSe solar cells under simulated AM 1.5, 100  $\text{mW cm}^{-2}$  illumination.

Precursor's Ga/(In+Ga)	$V_{oc}$ (V)	$j_{sc}$ ( $\text{mA cm}^{-2}$ )	$FF$ (%)	$\eta^a$ (%)	$R_s$ ( $\Omega$ $\text{cm}^2$ )	$R_{sh}$ ( $\Omega$ $\text{cm}^2$ )
0.00	0.392	26.36	42.02	<b>4.34±0.15</b>	12.71	1261.39
0.15	0.531	22.78	64.61	<b>7.81±0.18</b>	0.85	348.23
0.20	0.579	23.44	60.11	<b>8.15±0.12</b>	2.12	177.23
0.25	0.582	16.61	65.82	<b>6.36±0.09</b>	1.58	655.84
0.30	0.597	16.43	63.9	<b>6.27±0.21</b>	2.66	535.85
Optimized solar cell without ARC (0.2)	0.619	23.37	70.73	<b>10.22±0.30</b>	1.43	10274.8
with ARC (0.2)	0.621	24.29	69.84	<b>10.54±0.28</b>	1.66	949.48

<sup>a</sup> The standard deviation of cell efficiency is based on the data of 9 cells.

A single layer Mo-coated SLG substrate was utilized to prepare the non-optimized solar cells as shown in Table 2. Subsequently, we found that double layer Mo-coated SLG substrate showed better adhesion properties between Mo and CIGSSe films, and a very thin MoSe<sub>2</sub> layer was observed after selenization. Therefore, using the double layer Mo substrate an

optimized solar cells was found to be at  $\text{Ga}/(\text{In}+\text{Ga}) = 0.20$ . Solar cell made of an optimized CIGSSe film of  $\text{Ga}/(\text{In}+\text{Ga}) = 0.20$  shows excellent PCE  $\eta = 10.22\%$ ,  $V_{\text{oc}} = 0.619 \text{ V}$ ,  $j_{\text{sc}} = 23.37 \text{ mA cm}^{-2}$ , and  $FF = 70.73\%$  under AM 1.5,  $100 \text{ mW cm}^{-2}$  illumination (Table 2 and Fig. 4). Clearly, the optimized device demonstrates significant improvement in  $FF$  that may result from reduced carrier recombination and/or low series resistance. The much suppressed carrier recombination in the narrow space charge region is related to the quality of CIGSSe absorber layer, which generally increases the  $V_{\text{oc}}$  and  $FF$  of device. In addition, the better electronic properties may lead to large shunt resistance ( $R_{\text{sh}}$ ) and low series resistance ( $R_{\text{s}}$ ) as shown in Table 2. Several order lower  $R_{\text{sh}}$  (589 Ohms) than our observed value as shown in Table 2 has been reported in CIGSSe solar cells by Guo *et al.*, suggesting that the improved  $FF$  resulting from improved diode characteristics.<sup>51</sup> When an anti-reflection polymer film (ARC) was placed onto the optimized solar cells to reduce the reflection loss, higher  $j_{\text{sc}}$  consistent with the enhanced IPCE spectra was observed which eventually led to the PCE of 10.54% as shown in Figure 4.

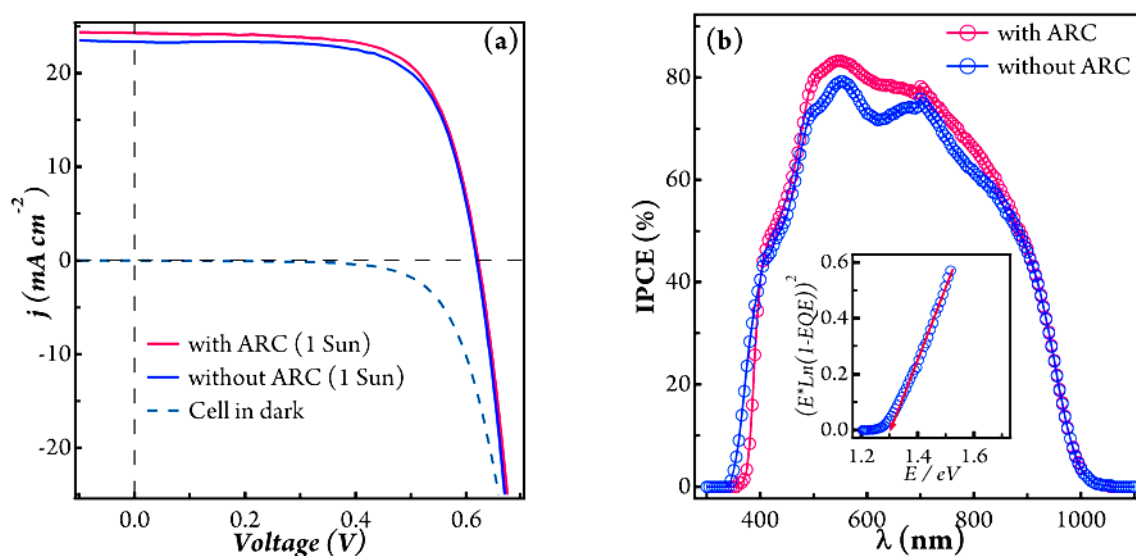


**Figure 4.** Shows  $j$ - $V$  characteristics (a), and IPCE spectra (b) of an optimized solar cell made of CIGSSe thin film with  $\text{Ga}/(\text{Ga}+\text{In}) = 0.20$ . The usage of an anti-reflection polymer film (ARC) enhances the light harvesting efficiency and photocurrent response of solar cells as observed from upward shift of IPCE spectra.

To the best of our knowledge, the device efficiency of 10.54% is the highest among the spray-pyrolysis-based CIGSSe thin film solar cells to date. The spray-pyrolysis technique has the potential to prepare CIGS thin films with large and uniform area. It should also be noted

that the highest obtained  $j_{sc}$  is approximately 23.5% with the best condition because of 1.15  $\mu\text{m}$  thickness CIGSSe film. Therefore, the film thickness could be doubled to increase light absorption and subsequent charge separation. To further enhance the charge separation of the solar cells, much efforts are needed to enhance the crystallinity of the CIGSSe thin films.

## Conclusions

The  $\text{Cu(In,Ga)(S,Se)}_2$  thin films was prepared by spray-pyrolysis of aqueous precursor solutions onto Mo-coated soda-lime glass. The use of water as solvent makes the film preparation method very facile and non-toxic, and the films are free of carbon impurity. The properties of CIGSSe thin films were modified by successful incorporation of Ga. The grown films were pure which is much desired for solar cell application. Optimized solar cells made of CIGSSe thin films exhibited significantly higher  $FF$  and  $V_{oc}$  which eventually resulted in power conversion efficiencies of 10.54%.

## Acknowledgements:

This work is supported by NTU-HUJ-BGU Nanomaterials for Energy and Water Management Programme under the Campus for Research Excellence and Technological Enterprise (CREATE), that is supported by the National Research Foundation, Prime Minister's Office, Singapore. Financial support from Singapore-Berkeley Research Initiative for Sustainable Energy (SinBeRISE) CREATE Programme and A\*STAR SERC Printed Photovoltaic Program (Grant No. 1021700143). The Israel National Nanotechnology Initiative is gratefully acknowledged.

## References

1. M. A. Green, K. Emery, Y. Hishikawa, W. Warta and E. D. Dunlop, *Prog. Photovoltaics Res. Appl.*, 2014, 22, 1-9.
2. C. Adrian, R. Patrick, P. Fabian, B. Patrick, R. U. Alexander, F. Carolin, K. Lukas, K. Debora, G. Christina, H. Hagendorfer, J. Dominik, E. Rolf, N. Shiro and N. T. Stephan Buecheler and Ayodhya, *Nat. Mater.*, 2012, 12, 1107-1111.
3. I. Repins, M. A. Contreras, B. Egaas, C. DeHart, J. Scharf, C. L. Perkins, B. To and R. Noufi, *Prog. Photovoltaics Res. Appl.*, 2008, 16, 235-239.
4. H. Liang, U. Avachat, W. Liu, J. van Duren and M. Le, *Solid State Electron.*, 2012, 76, 95-100.

5. A. T. Barrows, A. J. Pearson, C. K. Kwak, A. D. F. Dunbar, A. R. Buckley and D. G. Lidzey, *Energy Environ. Sci.*, 2014, 7, 2944-2950.
6. A. N. Tiwari, D. K. Pandya and K. L. Chopra, *Thin Solid Films*, 1985, 130, 217-230.
7. M. Krunks, O. Bijakina, V. Mikli, H. Rebane, T. Varema, M. Altosaar and E. Mellikov, *Sol. Energ. Mat. Sol. C.*, 2001, 69, 93-98.
8. D.-Y. Lee and J. Kim, *Thin Solid Films*, 2010, 518, 6537-6541.
9. M. Krunks, O. Kijatkina, A. Mere, T. Varema, I. Oja and V. Mikli, *Sol. Energ. Mat. Sol. C.*, 2005, 87, 207-214.
10. S. Ikeda, M. Nonogaki, W. Septina, G. Gunawan, T. Harada and M. Matsumura, *Catal. Sci. Technol.*, 2013, 3, 1849-1854.
11. N. D. Sankir, E. Aydin, M. Sankir and A. Bozbey, *J. Mater. Proc. Technol.*, 2014, 214, 1879-1885.
12. A. Erkan, D. S. Nurdan, U. Hulya and E. Uluer, *Int. J. Renew. Energy Res.*, 2012, 2, 491-496.
13. I. Oja, M. Nanu, A. Katerski, M. Krunks, A. Mere, J. Raudoja and A. Goossens, *Thin Solid Films*, 2005, 480-481, 82-86.
14. M. Krunks, O. Kijatkina, H. Rebane, I. Oja, V. Mikli and A. Mere, *Thin Solid Films*, 2002, 403-404, 71-75.
15. Y. Cai, J. C. W. Ho, S. K. Batabyal, W. Liu, Y. Sun, S. G. Mhaisalkar and L. H. Wong, *ACS Appl. Mater. Interfaces*, 2013, 5, 1533-1537.
16. S. J. Park, J. W. Cho, J. K. Lee, K. Shin, J.-H. Kim and B. K. Min, *Prog. Photovoltaics Res. Appl.*, 2014, 22, 122-128.
17. D. B. Mitzi, M. Yuan, W. Liu, A. J. Kellock, S. J. Chey, V. Deline and A. G. Schrott, *Adv. Mater.*, 2008, 20, 3657-3662.
18. Y. Xie, H. Chen, A. Li, X. Zhu, L. Zhang, M. Qin, Y. Wang, Y. Liu and F. Huang, *J. Mater. Chem. A*, 2014, 2, 13237-13240.
19. Y. Xie, Y. Liu, Y. Wang, X. Zhu, A. Li, L. Zhang, M. Qin, X. Lu and F. Huang, *Phys. Chem. Chem. Phys.*, 2014, 16, 7548-7554.
20. G. Wang, S. Wang, Y. Cui and D. Pan, *Chem. Mater.*, 2012, 24, 3993-3997.
21. W. Liu, D. B. Mitzi, M. Yuan, A. J. Kellock, S. J. Chey and O. Gunawan, *Chem. Mater.*, 2009, 22, 1010-1014.
22. W. Wang, S.-Y. Han, S.-J. Sung, D.-H. Kim and C.-H. Chang, *Phys. Chem. Chem. Phys.*, 2012, 14, 11154-11159.
23. C.-H. Chung, B. Bob, B. Lei, S.-H. Li, W. W. Hou and Y. Yang, *Sol. Energ. Mat. Sol. C.*, 2013, 113, 148-152.
24. S. Jeong, B.-S. Lee, S. Ahn, K. Yoon, Y.-H. Seo, Y. Choi and B.-H. Ryu, *Energy Environ. Sci.*, 2012, 5, 7539-7542.
25. V. A. Akhavan, B. W. Goodfellow, M. G. Panthani, D. K. Reid, D. J. Hellebusch, T. Adachi and B. A. Korgel, *Energy Environ. Sci.*, 2010, 3, 1600-1606.
26. V. A. Akhavan, T. B. Harvey, C. J. Stolle, D. P. Ostrowski, M. S. Glaz, B. W. Goodfellow, M. G. Panthani, D. K. Reid, D. A. Vanden Bout and B. A. Korgel, *ChemSusChem*, 2013, 6, 481-486.
27. M. Kar, R. Agrawal and H. W. Hillhouse, *J. Am. Chem. Soc.*, 2011, 133, 17239-17247.
28. Q. Guo, S. J. Kim, M. Kar, W. N. Shafarman, R. W. Birkmire, E. A. Stach, R. Agrawal and H. W. Hillhouse, *Nano Lett.*, 2008, 8, 2982-2987.

29. T. K. Todorov, O. Gunawan, T. Gokmen and D. B. Mitzi, *Prog. Photovoltaics Res. Appl.*, 2013, 21, 82-87.
30. A. R. Uhl, C. Fella, A. Chirilă, M. R. Kaelin, L. Karvonen, A. Weidenkaff, C. N. Borca, D. Grolimund, Y. E. Romanyuk and A. N. Tiwari, *Prog. Photovoltaics Res. Appl.*, 2012, 20, 526-533.
31. S. Ahn, K. Kim, A. Cho, J. Gwak, J. H. Yun, K. Shin, S. Ahn and K. Yoon, *ACS Appl. Mater. Interfaces*, 2012, 4, 1530-1536.
32. J. C. W. Ho, T. Zhang, K. K. Lee, S. K. Batabyal, A. I. Y. Tok and L. H. Wong, *ACS Appl. Mater. Interfaces*, 2014, 6, 6638-6643.
33. Se Han Kwon, Doo Youl Lee and Byung Tae Ahn, *J. Korean. Phys. Soc.*, 2001, 39, 655-660.
34. M. A. Contreras, K. Ramanathan, J. AbuShama, F. Hasoon, D. L. Young, B. Egaas and R. Noufi, *Prog. Photovoltaics Res. Appl.*, 2005, 13, 209-216.
35. S. Ahn, K. H. Kim, J. H. Yun and K. H. Yoon, *J. Appl. Phys.*, 2009, 105, 113533– 113537.
36. F. B. Dejene, *Sol. Energ. Mat. Sol. C.*, 2009, 93, 577-582.
37. F. B. Dejene and V. Alberts, *J. Phys. D: Appl. Phys.*, 2005, 38, 22.
38. M. Venkatachalam, M. D. Kannan, S. Jayakumar, R. Balasundaraprabhu and N. Muthukumarasamy, *Thin Solid Films*, 2008, 516, 6848-6852.
39. W. N. Shafarman, R. Klenk and B. E. McCandless, *J. Appl. Phys.*, 1996, 79, 7324-7328.
40. M. Park, S. Ahn, J. H. Yun, J. Gwak, A. Cho, S. Ahn, K. Shin, D. Nam, H. Cheong and K. Yoon, *J. Alloys Compd.*, 2012, 513, 68-74.
41. C. Rincón and F. J. Ramírez, *J. Appl. Phys.*, 1992, 72, 4321-4324.
42. W. Witte, R. Kniese and M. Powalla, *Thin Solid Films*, 2008, 517, 867-869.
43. H. Tanino, H. Deai and N. Hisayuki, *Jpn. J. Appl. Phys.*, 1993, 32, 436.
44. S. Roy, P. Guha, S. N. Kundu, H. Hanzawa, S. Chaudhuri and A. K. Pal, *Mater. Chem. Phys.*, 2002, 73, 24-30.
45. C. Rincón, S. M. Wasim, G. Marín, J. M. Delgado, J. R. Huntzinger, A. Zwick and J. Galibert, *Appl. Phys. Lett.*, 1998, 73, 441-443.
46. A. Cho, S. Ahn, J. Ho Yun, J. Gwak, S. Kyu Ahn, K. Shin, H. Song and K. Hoon Yoon, *Sol. Energ. Mat. Sol. C.*, 2013, 109, 17-25.
47. S. N. Qiu, L. Li, C. X. Qiu, I. Shih and C. H. Champness, *Sol. Energ. Mat. Sol. C.*, 1995, 37, 389-393.
48. L. L. Hench and J. K. West, *Chem. Rev.*, 1990, 90, 33-72.
49. Y. Oh, K. Woo, D. Lee, H. Lee, K. Kim, I. Kim, Z. Zhong, S. Jeong and J. Moon, *ACS Appl. Mater. Interfaces*, 2014, 6, 17740-17747.
50. T. Dullweber, O. Lundberg, J. Malmström, M. Bodegård, L. Stolt, U. Rau, H. W. Schock and J. H. Werner, *Thin Solid Films*, 2001, 387, 11-13.
51. Q. Guo, G. M. Ford, R. Agrawal and H. W. Hillhouse, *Prog. Photovoltaics*, 2013, 21, 64-71.